# A novel UAV-based ultra-light weight spectrometer for field spectroscopy

A. Burkart, S. Cogliati, A. Schickling and U. Rascher

***Abstract*—A novel hyperspectral measurement system for UAVs in the VIS/NIR range (350-800 nm) was developed based on the Ocean Optics STS microspectrometer. The ultralight device relies on small open source electronics and weighs ready to fly 216 g. The airborne spectrometer is wirelessly synchronized to a second spectrometer on the ground for simultaneous white reference collection. In this study the performance of the system was investigated and specific issues like dark current correction or second order effects were addressed. Full width at half maximum (FWHM) was between 2.4 – 3.0 nm depending on the spectral band. The functional system was tested in flight at 10 m altitude against a current field spectroscopy gold standard device ASD Field Spec 4 over an agricultural site. A highly significant correlation ($r^2 > 0.99$) was found in reflection comparing both measurement approaches. Furthermore the aerial measurements have a six times smaller standard deviation than the hand held measurements. Thus, the present spectrometer opens a possibility for low-cost but high-precision field spectroscopy from UAVs.**

***Index Terms*— Hyperspectral sensors, Remote sensing, Unmanned aerial vehicles, Vegetation, Calibration**

## I. Introduction

Field spectroscopy as well as hyperspectral remote sensing (RS) are common techniques to gain an insight on land cover beyond the human eye. Handmade ground measurements and on a larger scale air- and spaceborne spectroscopy are common investigation methods in the field of geology, geography and environmental science [1-3]. A major field in RS is the investigation of vegetation, which started in the 70th using spectral band indices like the NDVI. Currently RS evolves to a powerful proxy for plant investigation parameters [4]. Present studies show the utility of various parameters derived from hyperspectral data on plants like water [5] and chlorophyll content [6] as well as marker for diseases [7] or even insights in the photosynthetic apparatus by the retrieval of sun induced fluorescence [8]. Thus hyperspectral measurements are of high interest for observation of natural habitats and crop management. For this purpose continuous and automated measurement on single plots [9] and mapping of large areas with a given spatial resolution are needed. For continuous measurements, progress was recently made with the development of an autonomous hyperspectral system measuring the reflection over alpine grassland during a whole vegetation period [10]. On the other side a large number of studies were conducted on spectral imaging of whole agricultural sites with high spatial resolution using manned aircrafts [11-13] or different kind of unmanned aerial vehicles (UAV) [14, 15]. With the emerging development of small versatile UAVs their use in RS of vegetation offers simple and affordable observation from the air. Leading the field in spectral imaging of vegetation by UAVs, Zarco-Tejada et al. [16-18] demonstrated the feasibility of the technique for plant monitoring. On the technology side progress is expected on the development of miniature sensors to further enhance the performance of unmanned remote sensing platforms [19, 20]. Compared to well-proven field spectroscopy approaches the use of UAV based sensors is tempting due to their great degree of automation and fast throughput. However several issues still remain in the use of the acquired spectral data like Bidirectional Reflection Distribution Function (BRDF) [21], accurate atmospheric correction, adequate calibration procedures and the ease of use under various environmental conditions. Once these issues are solved, it will open up the opportunity to accurate investigation of common and advanced hyperspectral methods. An example is the sun induced fluorescence retrieval, which relies on highly accurate measurements [22] which are based on distinct knowledge about the characteristics of target, sensor and atmosphere.

To address these issues, in this paper we reduced the UAV based hyperspectral measurements to a single point spectrometer to provide a basic tool for the investigation of effects in field spectroscopy and its upscaling to airborne imaging platforms. Development, calibration and validation are described as well as the characterization of the novel Ocean Optics STS microspectrometer and the AscTec Falcon-8 as an airborne platform.

## II. Description of the UAV based spectrometer

*Principle of measurements*: The UAV based hyperspectral system is able to measure spectral radiance/reflectance over selected targets. It is based on an UAV carried air unit (AIR) and a ground unit (GND) both equipped with a STS-VIS microspectrometer (Ocean Optics, Dunedin, FL, USA). Technical details of the spectrometers units are reported in Table 1. The AIR unit is placed over the point of interest by

This work was supported by EFRE in the frame of CROP.SENSe.net.

A. Burkart, A. Schickling and U. Rascher are with the Institute of Bio- and Geosciences, IBG-2: Plant Sciences, Forschungszentrum Jülich GmbH,Leo-Brandt-Str., 52425 Jülich, Germany (e-mail: an.burkart@fz-juelich.de).

S. Cogliati is with the Remote Sensing of Environmental Dynamics Laboratory, DISAT, Università degli Studi Milano-Bicocca, Piazza della Scienza 1, Milan, Italy.

the UAV and measures the upwelling radiance while the GND unit acquires the sun irradiance over a white reference. During the technical implementation phase issues with dark current, calibration and a second order effect arose with the spectrometer and were solved before a validation experiment was conducted.

*Technical implementation*: Construction of both units was aimed towards simplicity, small weight and low costs. The AIR unit consists of the following components 1. STS microspectrometer; 2. Microcontroller (Seeeduino Stalker, Seeedstudio, Shenzhen, China) for data acquisition and wireless communication (Xbee-Pro, Digi International, Minnetonka, NM, USA); 3. Stable power regulation; 4. Lithium Polymer battery. The microcontroller listens to commands via the wireless interface and controls the spectrometer. Acquired spectra are saved to a micro SD. Due to RAM limitations of the microcontroller, spectra were recorded with a spectral binning of 4 resulting in 256 pixels. The firmware performing the required tasks was written using the open source platform Arduino [23]. The AIR unit itself is fully independent from the UAV and can also be used without the flying platform. Rugged cases for AIR and GND unit were constructed using a 3D printer (Mendel Prusa, www.reprap.org ) [24]. The weight of the operational AIR unit including battery is 216 g.

The GND unit establishes the wireless connection to the AIR unit and performs the reference measurements. It consists of: 1. STS microspectrometer 2. Xbee wireless modul. The ground unit is also connected to a field notebook that runs a graphical user interface (GUI) to control the entire system (AIR and GND). The GUI, written in the java based, platform independent, open source language Processing [25], provides simple access to control both spectrometers by mouse or keyboard commands. The software also includes post-processing functions for the output of fully corrected data. During flight the software allows the preliminary visualization of the spectra gathered by both units.

TABLE I
UAV SPECTROMETER DATASHEET

| | |
|---|---|
| Spectrometer | Ocean Optics STS-VIS |
| Spectral Range | 338 nm - 824 nm |
| Dynamic Range | 14 bit |
| Pixels | 1024 |
| Field of View | 12° |
| FWHM | 3 nm |
| Integration Time | 10 µs - 10 s |
| Battery life | 2 h |
| Wireless Range | >300 m |
| Weight (Air Unit) | 216 g |

The flying platform used in this study was an AscTec Falcon-8 (Ascending Technologies GmbH, Krailing, Germany) which is an eight motor rotary wing UAV with various stabilization systems. We used a camera adapter originally designed for a thermal camera. This adapter is stabilized to an adjusted angle, which can be specified during flight. It features a small RGB camera streaming a live video to the radio control, which simplifies the accurate aiming of the spectrometer. Furthermore the UAV has the capability to follow navigation points autonomously and to hover over a point of interest to allow for a long spectrometer integration time.

## III. DATA PROCESSING-CHAIN

*Dark current (DC) removal*: DC measurements are not possible during flight operations. Moreover STS microspectrometers do not have the "so-called" black pixels, sometimes present in spectrometers, to account for DC without the use of mechanical shutters in front of the instruments foreoptics. As the DC is a function of sensor temperature and integration time (IT) it can substantially change during operation. To correct target spectra during flight we characterised the DC influence in relation to integration time and sensor temperature [26].

DC was recorded in a laboratory considering a range of temperatures between 14°C to 34°C which represent the typical temperatures during field measurements. Several levels of integration time from 300 ms to 2000 ms have been selected. Measurements were performed automatically and temperature was detected by the on chip thermometer in the ELIS-1024 linear image photo sensor used in the STS microspectrometer.

*Second Order Effect*: The STS VIS microspectrometers have a second order effect which introduces an additional stray light signal measured at the double of the real incoming wavelength [13]. Pixels between 676 nm and 823 nm are affected by this stray light due to light measured at the pixels between 338 nm and 412 nm. This effect was characterized using a monochromator (Lambda 950 Spectrophotometer, Perkin Elmer, Waltham, Massachusetts, US) illuminating with a narrow bandwidth of 4 nm and saving the spectra for analysis. The integration time was adapted to prevent the spectrometer from saturation and to compare the strength of the illuminating light and the strength of the stray light induced by the second order effect.

*Instrument calibration*: Field spectroscopy techniques aimed at reflectance measurements do not require the absolute spectral and radiometric calibration of spectrometers in physical units. In fact, the reflectance factor is typically determined rationing the target and the white reference measurements collected with the same illumination (i.e. irradiance) and instrumental conditions (i.e. integration time). The UAV system relies on two different spectrometers to collect target and reference measurements. This experimental setup requires a proper spectral/radiometric crosscalibration of the instruments. Factory spectral calibration factors and instruments FWHM were controlled with the SpecCal tool

[27] which allows evaluating instruments performances comparing field measurements with radiances simulated by the atmospheric radiative transfer code Modtran5 [28]. Radiometric calibration was inferred comparing STS spectrometers with a well calibrated ASD FieldSpec PRO 4 (Analytical Spectral Devices, Inc., Boulder, Colorado, US). Simultaneous measurements were collected in such way that the spectrometer´s field of view were totally overlapping on the white reference panel (Spectralon, Labsphere ,Inc., North Sutton, NH, US). A number of spectra were collected at different Solar Zenith Angles (SZA) to provide measurements covering different light levels. STS spectra were resampled to the ASD FieldSpec bands, thus a linear relationship between ASD radiance values ($L_{ASD}$) and STS digital counts at different light levels, normalized for the different instrument integration time (IT), was estimated for the 1024 spectral bands. The slope of the linear models represents the radiometric gain factors at different wavelengths that will successively be used to convert instrument relative values to absolute radiance values (eq. 1).

$$L_{ASD} = \frac{counts}{IT * gains} \quad (1)$$

## IV. Field Measurements

Several test flights were performed to test the technical performance of the spectrometer and the UAV. After those successful preliminary flights a validation experiment was performed on 14 November 2012 over agricultural fields next to the research centre of Jülich (lat 50.896312, lon 6.426436). The illumination conditions were low, but because of a cloudless sky stable. Three different homogeneous targets 1. grassland 2. young wheat 3. bare soil were measured with the UAV spectrometer and at the same time with an ASD Field Spec 4 Pro. UAV measurements were conducted between 1:10 pm and 1:23 pm local time and each target was measured 8 times. The ground unit was placed in the center of the three targets. Flight altitude was 10 m over ground according to about 2 m diameter of the viewed spot. The observation angle was at nadir. The UAV was controlled manually and flown in transects over the targets during acquisition (Fig. 1).

Due to the low illumination integration time ranged between 473 and 481 ms and was automatically optimized. The optimization of the dynamic range of the spectrometer was performed by test measurements of the GND unit and adapted to the AIR unit.

ASD measurements were conducted with a pistolgrip about 1 m above the surface. 75 measurements were acquired along a transect over each target. Every 25 measurements irradiance was measured over a white reference panel (Spectralon). ASD data collection took place between 1 pm and 2 pm.

Reflectance was calculated for the ASD data using the average of the white reference measurements recorded for each target. The UAV spectrometer reflectance was calculated using the white reference and upwelling irradiance of each data point after post processing, including dark current correction and calibration. Overall reflectance of the targets was determined for the two datasets with mean and standard deviation.

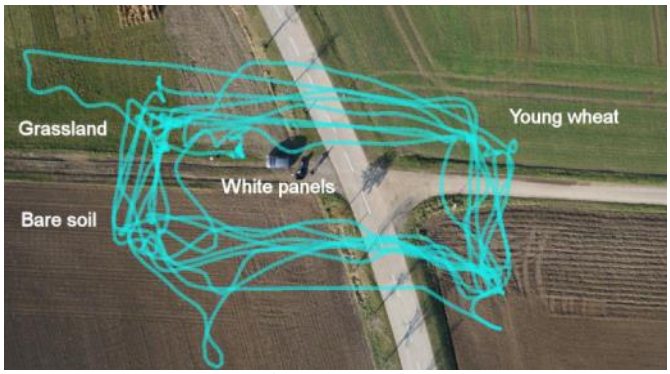

Fig. 1. Experimental site and flight pattern of the Falcon-8 UAV during the hyperspectral measurement collection. Grassland, young wheat and bare soil were observed with the UAV spectrometer and the ASD field spec. White panels were placed in the center as indicated.

Statistical analysis was conducted using Excel 2002 (Microsoft Corp., Redmond, WA, US) and Graphpad Prism 4.0 (GraphPad Software Inc., La Jolla, CA, USA).

## V. Results:

*Dark current removal*: The DC measured at different integration times and at several stable temperature levels follows a linear function with $R^2 > 0.99$ (Fig 2.). Corresponding measurements were performed for both spectrometers (i.e. AIR/GND).

Measurements performed for single pixels with raising temperature (Fig 3.) and divided by integration time after subtraction of the baseline were fitted to an exponential function ($R^2 > 0.95$ for pixel 4 of the air unit). Each pixel showed a different temperature response in dark current

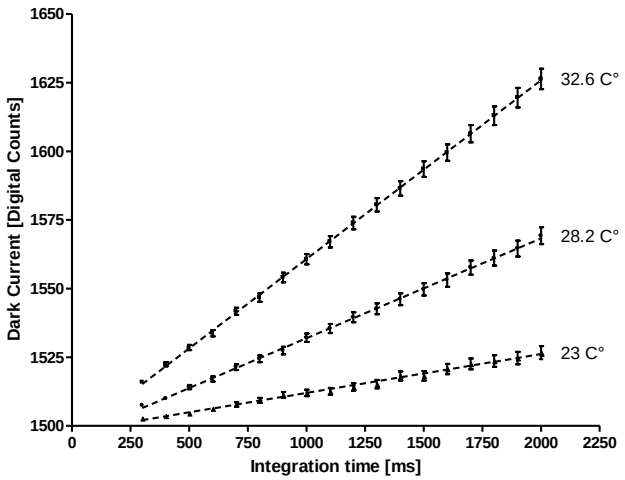

Fig. 2. Linear regression of dark current at three different detector temperatures and changing integration time. Dots and whiskers are mean values and standard deviations respectively for all spectral bands (n = 256).

leading to an overall $R^2 = 0.91$ for the AIR unit and $R^2 = 0.945$ for the GND unit. With these results the DC for the investigated integration times from 300 ms to 2000 ms and temperature levels from 14 °C to 34 °C could be estimated. With the fitted exponent function for the temperature (T) for each specific spectrometer and pixel (p) and the integration time (IT) the DC can be determined for every single pixel by the formula (2) where A, B and C are the constants of the fitted exponent function for each pixel.

$$DC_{[p]} = \left(A_{[p]} + B_{[p]} * e^{C_{[p]}*T}\right) * IT \quad (2)$$

To validate the methodology, this DC correction was applied to additional exemplary measurements at 33 °C. In addition we collected the true DC as measured with closed optics. The deviation from the actual measured DC was in average 2.39 digital counts (air unit) which is less than 0.02 % of the 14 bit dynamic range.

*Second order effect*: The effect of the stray light of the second order was determined for the wavelength from 340 nm to 410 nm of the AIR unit in 10 nm steps. The amount of second order straylight, induced by monochromatic light was

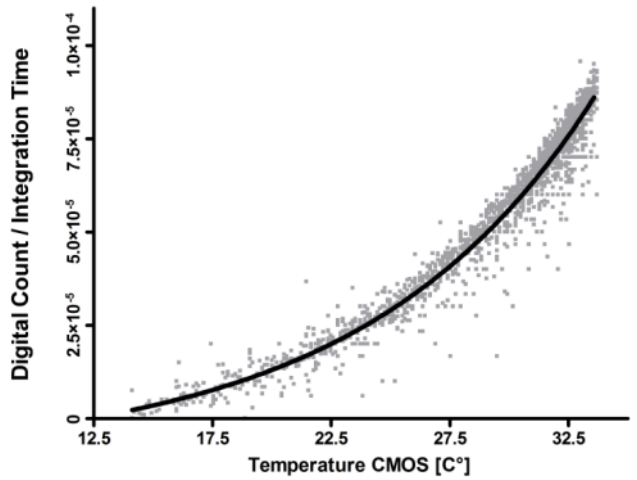


Fig. 3. Exponential regression of dark current dependency to raising detector temperature shown for Pixel 4 of the air unit´s STS microspectrometer (n = 1854, $R^2 = 0.9586$). Data was fitted with an exponent function $y=a+b*e^{cx}$).

determined for the investigated wavelengths (Fig 4.). These factors determining the amplitude of the undesired signal at the double wavelength showed a linear behaviour ($R^2$ = 0.9149).

*Instrument calibration*: Investigation of the spectral performance of AIR and GND unit with the SpecCal tool resulted in FHWM less than 3 nm and a small spectral shift as seen in table 2. By comparing the white reference measurements of the AIR and GND unit with the radiometrically calibrated ASD spectra a transformation vector for each spectrometer was calculated. This vector was used to translate digital count measurements to physical units (eq. 1) and to crosscalibrate GND and AIR.

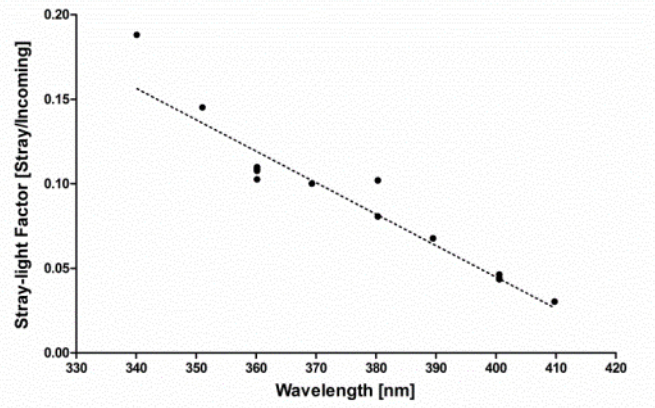


Fig. 4. Linear regression of the measured second order effect and its strength compared to the inducing wavelength (n = 17, $R^2 = 0.9149$).

*Field Measurements*: Reflection over the 3 different targets (grassland, wheat, soil) was calculated and analyzed for ASD and the UAV spectrometer. Mean reflection spectra of both devices followed the same pattern with minor differences in the beginning and end of the spectra. The most significant

TABLE II
ACCURACY OF SPECTROMETERS USED IN THIS STUDY

| Device | Spectral Range [nm] | Spectral Shift [nm] | FWHM [nm] |
|---|---|---|---|
| ASD | 350.00 - 1050.00 | -0.05 | 3.79 |
| GND | 337.65 - 824.30 | -0.05 | 2.30 |
| AIR | 337.65 - 824.30 | 0.15 | 3.00 |

difference to the actual reflection was seen in the $O_2$-A absorption band at 760 nm of the UAV spectrometer. Correlation of the reflection measurements of both systems

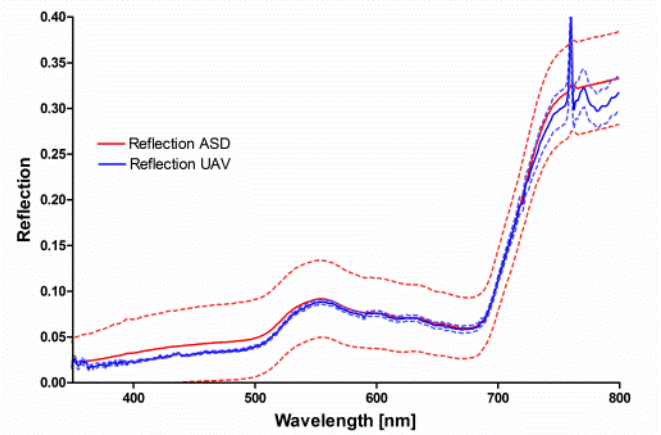


Fig. 5. Reflection over grassland measured by ASD field spec (n = 75) and UAV spectrometer (n = 8). Standard deviation is indicated by the dotted lines. Standard deviation on the other targets (wheat and soil) was similar high in ASD measurements and low in the UAV measurements.

was highly significant ($R^2$ = 0.9912). The three surfaces showed spatial heterogeneities such as vegetation patches, tire tracks and row seeding. The standard deviation of the UAV spectrometer´s measurements was smaller than in ASD data. This was caused by the much larger footprint of the UAV spectrometer. Over grassland ASD data varied with an average standard deviation in reflection of 4.1 % while the standard deviation with an average of 0.59 % of the UAV spectrometer measurements was 6 times smaller (Fig 5.).

## VI. Discussion:

The calibration and validation experiments performed on the UAV spectrometer have proven that high precision spectroscopic measurements can be performed using the miniaturized spectrometers. The modelled dark current correction showed good results but care must be taken for influence of the second order effect which may cause errors in the NIR. High uncertainties are present in the reflection calculated inside the atmospheric $O_2$-A absorption feature at 760 nm. This issue will be addressed in future development to enable the spectrometer to accurately retrieve the sun induced fluorescence. The STS microspectrometers performed well regarding their size, but are still outperformed in sensitivity and accuracy by other larger and heavier sensors such as the Ocean Optics HR4000 or the USB2000. Despite this the spectral accuracy is comparable to the VIS of the current gold standard device ASD Field Spec Pro 4. Comparative measurements over agricultural fields have shown a far lower standard deviation in the UAV spectrometer data due to the larger field of view, compared to the ASD Field Spec measurements. Moreover, the very fast acquisition procedure over large sites proves the approach as an useful complement for conventional field spectroscopy. Taking advantage of the system it will be used in upcoming airborne and satellite campaigns such as the new high performance hyperspectral sensor HyPlant, as the UAV allows easy acquisition of reference reflectance measurements over areas difficult to access. The opportunity of changing the angle of the spectrometer during flight also allows the use as a giant flying goniometer for the investigation of BRDF effects [29] especially in forest [30]. The UAV spectrometer without the flying platform is also as a fully autonomous device suitable for the use in constant monitoring. It draws very low energy and has a built-in battery and charge circuit that can be powered by a small solar array.

In the quickly evolving field of UAV based spectral imaging, we took a step towards high-precision field spectroscopy and built a basic tool for hyperspectral research. To lay a base for future experiments the sensor was properly characterized and possible sources of error like the second order effect were identified. With the UAV spectrometer the gap between field spectroscopy and airborne sensors is about to be closed.

## VII. Acknowledgment

The authors thank T. Burkart for the design and manufacture of the spectrometer cases.

## VIII. References

[1] E. J. Milton, M. E. Schaepman, K. Anderson, M. Kneubühler, and N. Fox, "Progress in field spectroscopy," Remote Sensing of Environment, vol. 113, pp. S92-S109, 2009.

[2] G. Vane and A. F. H. Goetz, "Terrestrial imaging spectrometry: current status, future trends," Remote Sensing of Environment, vol. 44, pp. 117-126, 1993.

[3] F. D. van der Meer and S. M. de Jong, Imaging Spectrometry: Basic Principles and Prospective Applications vol. 4: Springer, 2011.

[4] A. Bannari, D. Morin, F. Bonn, and A. Huete, "A review of vegetation indices," Remote sensing reviews, vol. 13, pp. 95-120, 1995.

[5] J. Penuelas, J. Pinol, R. Ogaya, and I. Filella, "Estimation of plant water concentration by the reflectance water index WI (R900/R970)," International Journal of Remote Sensing, vol. 18, pp. 2869-2875, 1997.

[6] D. Haboudane, J. R. Miller, N. Tremblay, P. J. Zarco-Tejada, and L. Dextraze, "Integrated narrow-band vegetation indices for prediction of crop chlorophyll content for application to precision agriculture," Remote Sensing of Environment, vol. 81, pp. 416-426, 2002.

[7] A. K. Mahlein, T. Rumpf, P. Welke, H. W. Dehne, L. Plümer, U. Steiner, et al., "Development of spectral indices for detecting and identifying plant diseases," Remote Sensing of Environment, vol. 128, pp. 21-30, 2013.

[8] M. Meroni, M. Rossini, L. Guanter, L. Alonso, U. Rascher, R. Colombo, et al., "Remote sensing of solar-induced chlorophyll fluorescence: Review of methods and applications," Remote Sensing of Environment, vol. 113, pp. 2037-2051, 2009.

[9] M. Balzarolo, K. Anderson, C. Nichol, M. Rossini, L. Vescovo, N. Arriga, et al., "Ground-based optical measurements at European flux sites: a review of methods, instruments and current controversies," Sensors, vol. 11, pp. 7954-7981, 2011.

[10] M. Meroni, A. Barducci, S. Cogliati, F. Castagnoli, M. Rossini, L. Busetto, M. Migliavacca, E. Cremonese, M. Galvagno, R. Colombo, and U. Morra di Cella "The hyperspectral irradiometer, a new instrument for long-term and unattended field spectroscopy measurements," Review of scientific instruments, vol. 82, pp. 43106-43106, 2011.

[11] R. Pu, M. Kelly, G. L. Anderson, and P. Gong, "Using CASI hyperspectral imagery to detect mortality and vegetation stress associated with a new hardwood forest disease," Photogrammetric Engineering and Remote Sensing, vol. 74, p. 65, 2008.

[12] D. Haboudane, J. R. Miller, E. Pattey, P. J. Zarco-Tejada, and I. B. Strachan, "Hyperspectral vegetation indices

and novel algorithms for predicting green LAI of crop canopies: Modeling and validation in the context of precision agriculture," Remote Sensing of Environment, vol. 90, pp. 337-352, 2004.

[13] J. Kuusk and A. Kuusk, "Autonomous lightweight airborne spectrometers for ground reflectance measurements," in Hyperspectral Image and Signal Processing: Evolution in Remote Sensing (WHISPERS), 2010 2nd Workshop on, 2010, pp. 1-4.

[14] J. J. Mitchell, N. F. Glenn, M. O. Anderson, R. C. Hruska, A. Halford, C. Baun, et al., "Unmanned Aerial Vehicle (UAV) Hyperspectral Remote Sensing for Dryland Vegetation Monitoring," 2012.

[15] J. Primicerio, S. F. Di Gennaro, E. Fiorillo, L. Genesio, E. Lugato, A. Matese, et al., "A flexible unmanned aerial vehicle for precision agriculture," Precision Agriculture, pp. 1-7, 2012.

[16] P. Zarco-Tejada, V. González-Dugo, and J. Berni, "Fluorescence, temperature and narrow-band indices acquired from a UAV platform for water stress detection using a micro-hyperspectral imager and a thermal camera," Remote Sensing of Environment, 2011.

[17] J. Berni, P. J. Zarco-Tejada, L. Suárez, and E. Fereres, "Thermal and narrowband multispectral remote sensing for vegetation monitoring from an unmanned aerial vehicle," Geoscience and Remote Sensing, IEEE Transactions on, vol. 47, pp. 722-738, 2009.

[18] J. Berni, P. Zarco-Tejada, L. Surez, V. González-Dugo, and E. Fereres, "Remote sensing of vegetation from uav platforms using lightweight multispectral and thermal imaging sensors," The International Archives of the Photogrammetry, Remote Sensing and Spatial Information Sciences, XXXVII, 2008.

[19] G. Rufino and A. Moccia, "Integrated VIS-NIR hyperspectral/thermal-IR electro-optical payload system for a mini-UAV," Infotech@ Aerospace, pp. 1-9, 2005.

[20] H. Saari, V. V. Aallos, A. Akujärvi, T. Antila, C. Holmlund, U. Kantojärvi, et al., "Novel miniaturized hyperspectral sensor for UAV and space applications," in SPIE Europe Remote Sensing, 2009, pp. 74741M-74741M-12.

[21] F. E. Nicodemus, "Directional reflectance and emissivity of an opaque surface," Applied Optics, vol. 4, pp. 767-773, 1965.

[22] A. Damm, A. Erler, W. Hillen, M. Meroni, M. E. Schaepman, W. Verhoef, et al., "Modeling the impact of spectral sensor configurations on the FLD retrieval accuracy of sun-induced chlorophyll fluorescence," Remote Sensing of Environment, vol. 115, pp. 1882-1892, 2011.

[23] M. Banzi, Getting started with Arduino: Make, 2008.

[24] R. Jones, P. Haufe, E. Sells, P. Iravani, V. Olliver, C. Palmer, et al., "RepRap–the replicating rapid prototyper," Robotica, vol. 29, pp. 177-191, 2011.

[25] C. Reas and B. Fry, "Processing. org," Processing. org, vol. 3, 2012.

[26] J. Kuusk, "Dark Signal Temperature Dependence Correction Method for Miniature Spectrometer Modules," Journal of Sensors, vol. 2011, 2011.

[27] M. Meroni, L. Busetto, L. Guanter, S. Cogliati, G. F. Crosta, M. Migliavacca, *et al.*, "Characterization of fine resolution field spectrometers using solar Fraunhofer lines and atmospheric absorption features," Applied optics, vol. 49, pp. 2858-2871, 2010.

[28] A. Berk, G. P. Anderson, P. K. Acharya, L. S. Bernstein, L. Muratov, J. Lee, *et al.*, "MODTRAN5: 2006 update," in Proc. SPIE, 2006, p. 62331F.

[29] F. N. G.J. Grenzdörffer, "UAV Based BRDF-Measurements of Agricultural surfaces with Pfiffikus," presented at the UAV-g 2011, Conference on Unmanned Aerial Vehicle in Geomatics,, Zurich, Switzerland, 2011.

[30] F. Fassnacht and B. Koch, "Review of forestry oriented multi-angular remote sensing techniques," International Forestry Review, vol. 14, pp. 285-298, 2012.